EXPERIMENTAL AND NUMERICAL APPLICATION ON BENDING RESISTANCE OF CONCRETE FILLED STEEL TUBE ARCH AT FIXED ENDS

ZHANG XIAO-NAN[1,2,3] *, SHAN REN-LIANG[1], QI CHENG-ZHI[2]

[1]*School of Mechanics and Civil Engineering, China University of Mining and Technology, Beijing, 100083, P.R. China;*
[2]*Beijing Future Urban Design High-Tech Innovation Center and 2011 Energy Conservation and Emission Reduction Collaborative Innovation Center, Beijing University of Civil Engineering and Architecture, Beijing, 100044, P.R. China;*
[3]*School of Civil Engineering, Hebei University of Engineering, Handan,056038, P.R. China*

Through the monitoring of the displacement of the middle accross section in concrete filled steel tube (CFST) arch with 0.26 rise-span ratio, which fixed at both ends under the condition of uniform loading, as well as the strain and the ultimate bearing capacity of outer steel pipe and inner core of concrete which combined with ABAQUS for simulation analysis of bending process. Meanwhile, based on the ABAQUS simulation software with cohesive elements as the main research method in the constitutive model of concrete was put forward. The actual simulating and experiment results shows that the local failure characteristics of core concrete of CFST arch is similar to those of uniaxial compression on concrete short columns, and there is only compressive stress exists among the middle accross section of CFST arch which causes the volume of the inflated burst when fixing at both ends. Moreover, there is no influence on the bearing capacity of the overall core concrete with and the load displacement curves, which proved the efficiency of the proposed method and the basis for the study of other components of CFST during the mine construction.

Keywords: *Bending experiment of CFST arch, ABAQUS, Cohesive elements, Constitutive model, Uniaxial compression experiment*

1. Introduction

The concrete-filled steel tubular (CFST) structure is a kind of composite supporting structure formed by pouring concrete into the steel pipe which is on the basis of making full use of the hoop effect of ferrule and the excellent pressure-bearing performance of the concrete. The core concrete plays the role of supporting the steel pipe and improving the stability of the steel pipe, the reaction of the steel pipe to the concrete can increase the bearing capacity of the concrete. It is mainly used in such as deep-seated roadway in soft strata, subway station, bridges and high-rise buildings and other structural projects [1-4].

Foreign application of steel tube concrete in mine roadway support is less, but domestic scholars presented the free torsional stiffness and flexural stiffness expressions in view of the steel-tube concrete arc arch theory, and also checked the free torsional stiffness and flexural rigidity of the circular and square section arch structures with ANSYS which analyzed on the characteristic value side-tilting buckling of cfst arc arch with different height-span ratio and steel-bearing ratio. At the same time, relevant scholars through the core concrete strain device to monitor the load in the uniform, under the different conditions of completely fixing the arch-foot, such as the influence ratio of vector to span, the strength of core concrete, the steel fiber parameters, the thickness of steel pipe, the size of the bending round steel and the different diameters on the bearing capacity of the arc-shaped arch specimen are analyzed. Therefore, there are some guiding significance for the application of CFST arch for the research on the bending and failure mechanism of CFST arch which affected by radial load in the condition of arc-arch end slip, as well as the analysis on axial compression and failure mechanism of core concrete[5-7].

This paper shows the bending test of CFST arch in the large-scale laboratory, through the monitoring the ultimate bearing capacity under the slippage of both ends with the condition of uniform loading, as well as the displacement of the middle across section and the strain of outer steel pipe and inner core of concrete which combined with ABAQUS for analysis on the bending process. Moreover, according to the measurement results, it is possible to analyze the relative velocity and variation of the relative displacement of the surrounding rock in the main surrounding roadway, so as to judge the supporting effect and the stability of the surrounding rock, and provide the basis for perfecting the supporting parameters.

2. Calculation of bending load in arch flat

The theoretical solution of CFST arch which is in the elastic state with structural mechanics

* Autor corespondent/*Corresponding author*,
E-mail: zxn863726147@163.com

analysis. However, when the steel pipe or core concrete enters the plastic state the CFST specimen has a large deformation which isn't satisfied with the basic assumption of structural mechanics, so the structural mechanics solution will no longer apply [8-10]. Moreover, the slippage at both ends of the arch will be considered under the radial load, which the anti-symmetry instability in will display in the plane as shown in Figure 1.

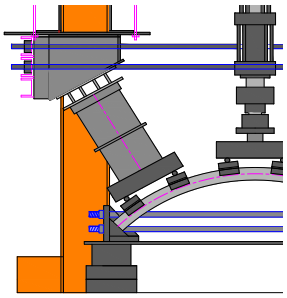

Fig.1 - Calculation diagram of the arch under uniform load.

Since the radial displacement and the corner of the fixed end of the CFST arch specimen are zero, the buckling differential equation of circular arch under radial load:

$$\frac{d^2v}{d\varphi^2}+v=-\frac{(qRv-M_0\sin\varphi/\sin\alpha)R^2}{E_sI_s+\alpha_0E_cI_c};$$

$$\therefore q=(n^2-1)\frac{E_sI_s+\beta_0E_cI_c}{R^3}; \quad (1)$$

$$n=18991.26e^{(-2\alpha/3.03)}+13.40e^{(-2\alpha/35.75)}+1.88 \quad (2)$$

Where: the pan ratio is 0.26, f=0.26*l*; The bending moment at the fixed end of the arch is M_0; Elastic modulus of steel is E_s=2.06×10^{11}Pa; Elastic modulus of concrete is E_c=3.25×10^{10}Pa; $f_{cu,k}$ is compressive strength of concrete cubes; The reduction factor β_0=0.8 which takes into account the cracking of the concrete when the member is bent; Hollow steel pipe moment of inertia is I_s; Core concrete moment of inertia is I_c, which are as follows:

$$I_s=\frac{\pi D^4}{64}-\frac{\pi d^4}{64}=\frac{\pi D^2}{64}\left(1-\frac{d}{D}\right)^4;\ I_c=\frac{\pi d^2}{64} \quad (3)$$

Where, Outside diameter of steel pipe is D; Inside diameter of steel pipe is d.

3. Experimental study on bearing capacity of CFST arch

3.1. Constituents of steel pipe and core concrete

The parameter settings of constituents of steel pipe :

$$\begin{cases}\sigma_s=E_s\varepsilon_s & \varepsilon_s\le\varepsilon_{e1}\\ \sigma_s=f_y & \varepsilon_{e1}\le\varepsilon_s\le\varepsilon_{e2}\\ \sigma_s=f_u-(f_u-f_y)(\varepsilon_{e3}-\varepsilon_s)^2/(\varepsilon_{e3}-\varepsilon_{e2})^2 & \varepsilon_{e2}\le\varepsilon_s\le\varepsilon_{e3}\\ \sigma_s=f_u & \varepsilon_s\ge\varepsilon_{e3}\end{cases} \quad (4)$$

Where: Elastic modulus of steel is E_s= 206Gpa; Yield strength of steel is f_y; Steel tensile strength is f_u, f_u=1.6f_y; The proportion of steel limit is f_p.

Table 1

Parameters of concrete plastic damage model

ρ/ kg·m^3	*λ*	*M*	*φ*/ °	*w*/ %	f_k/ *KPa*	*c*/ *KPa*	*E*/ *GPa*
2400	0.2	0.1	30	43.3	0.67	0.005	33

Where: *ρ* is density; λ is poisson's ratio; M is flow potential eccentricity; φ is swell angle; w is the ratio of biaxial isobaric to uniaxial strength ; f_k is second stress ratio; c is cosity coefficient; E is lastic modulus.

3.2. Design and manufacture of CFST arch

The CFST arch bending performance experiment performed in the structural laboratory of our school as shown in Figure 2, the laboratory is equipped with large-scale reactor bench and many different tonnage jacks, the experimental conditions are able to meet the experimental requirements and aims.

Fig.2 - The test bench and the pre-buried strain.

Considering the conditions both uniform loading and slippage at both ends of CFST arch, along the bracket vertical centerline and horizontal center line displacement sensor, combing with hydraulic jacks supporting the pressure sensor to collect the load. In this experiment, there are 9 specific displacement meters monitored displacement where distributed among the both end's supports and pads, middle across section, and 1/4 span section of the CFST arch, as shown in Figure 3.

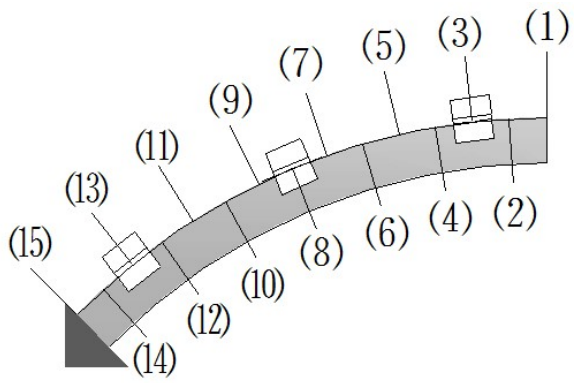

Fig.3 - Arrangement diagram of displacement meter.

3.3. Experimental steps

First, the midpoint of CFST arch is found and the overall specimen is assembled on the ground. Then, the strain gauges are attached and the overall specimen with slip supports is lifted to the experimental platform. In the end, connect the strain gauge wire, install the displacement sensor and adjust the hydraulic jacks in place, everything is ready for the beginning of the experiment.

Adding and recording the loads and data according to the steps of experiments design. After the whole test, hanging the CFST arch on the ground and timely monitoring the late data.

3.4 Experimental results analysis

The steel pipe at both ends of the CFST arch with 0.26 span ratio which can be seen to be significantly thicker. As the specimen is uniformly compressed, the radius of curvature of the specimen increases, and the radius of curvature is no longer the same. The CFST arch is relatively severe by the straightening of the arc, as shown in Figure 4.

Fig.4 - Overall deformation of circular arch with 0.26 rise-span ratio.

3.5. Experimental analysis of curved bending of CFST arch

The CFST arch research from beginning of load to the whole process of bending and breaking, and analyzed the deformation of the CFST arch is fixed at both ends. After each loading step, the displacements and loads of the across section and arch among the CFST specimen, the data plotted as the load-displacement curve which is shown in Figure. 5.

According to the load-displacement curve, the arc arch deformation can be divided into four stages: compaction stage, elastic deformation stage, elastic-plastic deformation stage and plastic

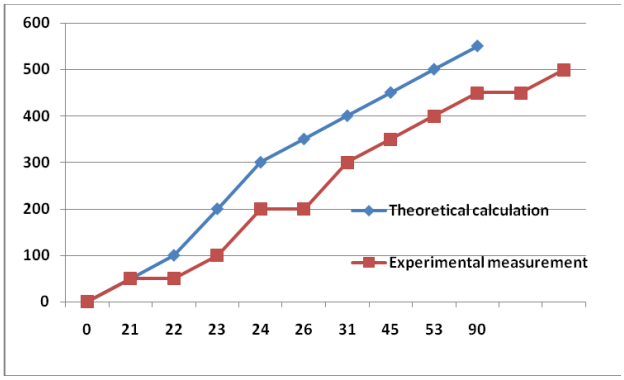

Fig.5 - Load-displacement curve.

deformation stage [11].

Therefore, the yield and ultimate loads of the specimen are reduced with the increase of the slip at both ends of the CFST arch. Which means the smaller of the distance between the arch is, the greater of the ultimate bearing capacity of CFST arch will be, and the deformation ability to resist bending will better.

4. Numerical analysis of CFST arch

4.1 Mechanics model and boundary constraint

The indoor experiment can only monitor the bearing capacity, displacement and strain of the CFST arch. But the stress distribution, axial force and bending moment of the CFST arch are analyzed by means of numerical simulation. Therefore, ABAQUS simulation software is used to analyze the stress, axial force, bending moment and load-displacement curve of concrete-filled steel tube arch [12-16]. The finite element model is established in accordance with the actual situation of the experiment. Along the axis of the CFST arch carried out the uniform loading, fixed at the both ends of the specimen, and restrained the deformation outside the plane, the mechanical model as shown in Figure 6. Compared the loading with experimental, which can be more stable with computer simulation, and easy to be controlled. Therefore, the 0-400kN range of loading in each rank of pad which simulated as 50kN, after 400kN which simulated as 25kN.

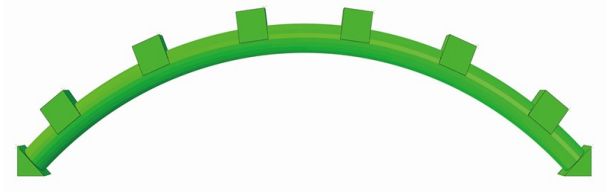

Fig.6 - Circular arch mechanical model.

The accuracy of finite element simulation is highly dependent on the type of unit. In the case of elasto-plastic simulation of CFST arch, taking into account the larger strain, displacement and bending moment, choosing the integral unit is easy to produce volume self-locking phenomenon. Therefore, the type of reduced integral unit

Fig.7 - The cloud of 1# test block steel tube.

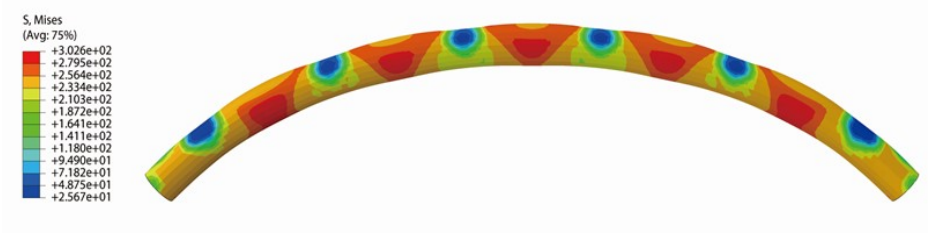

Fig.8 - The cloud of 2# test block steel tube.

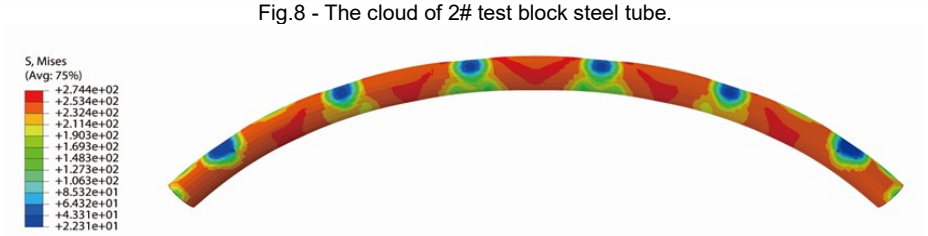

Fig.9 - The cloud of 3# test block steel tube.

(C3D8R) which selected as the simulation unit. Then, the nonlinear analysis on the larger area of the plastic deformation rule which could improve the accuracy of the solution.

4.2 Stress distribution law of steel tube surface

The steel pipe surface will be buckled and drum packaged during the CFST arch loading, which is obviously shown general stress concentration in this area.

When the load is 50kN three specimens of the steel pipe surface stress distribution are shown in Figures 7 - 9.

Compared with the above three specimens after the end of CFST arch slip, according to the Mises comprehensive cloud inages of steel surface the conclusions are as follows:

(1)The concentration phenomenon which are appeared in the cross section and arch foot of the three specimens, and the specimen of 2# and 3# are more obviously and larger than 1#;

(2)The loading points among the three specimens become stress reduction zones which due to the wrapping of the pads, as well as the area between the loading points of the specimen of 2# and 3#. Although the area between the loading points of the specimen of 1# is stress increase zone, but the stress of the specimen of 2# and 3# is larger than1#.

4.3 Stress distribution law of core concrete

As the concrete is anisotropic material, in the post-processing of ABAQUS software, the Mises-S11 cloud shows the transverse force distribution of the specimen, if S11 is positive, it represents for lateral tension, while S11 is negative, which means the lateral compression.

When the load is 50kN, the stress distribution of S11 in the vertical section of the core concrete of the three specimens are shown in Figures 10 - 12.

Through the analyzed above, it is found that when the load of the specimen is 50kN, the core concrete of 1 # specimen is fully pressurized, and the largest compressive stress where distributed in the core of the circular arch. The pressured area and tensioned area which exists in vertical profile of core concrete of 2# and 3# along with arch axis previously.

In addition, the slippage of CFST arch can “enlarge” the ability from the load to the core concrete, so that the core concrete inside the steel pipe under pressure. Keep on loading, the end constraints of the three specimens are treated as fixed conditions. The stress area of the core concrete is gradually reduced until the specimen is yielded and destroyed, in the end the core concrete is completely compressed.

4.4. Simulation of uniaxial compression of concrete test block

It is found that there is only compressive stress in the cross section of the core concrete in the 1 # CFST arch when fixed the both ends, as shown in Figure 13.

It is shown that the core concrete is crushed and inflated under the action of pressure and bending under the condition that the ends of the specimen is completely fixed. The local failure characteristic is similar to the uniaxial compression on CFST specimen, as shown in Figure 14.

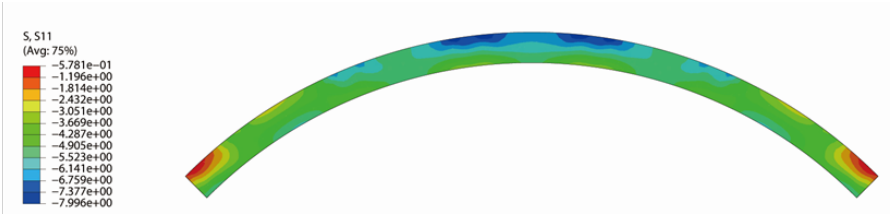

Fig.10 - The distribution of the stress from S11 vertical section of 1# test block.

Fig.11 - The distribution of the stress from S11 vertical section of 2# test block.

Fig.12 - The distribution of the stress from S11vertical section of 3# test block.

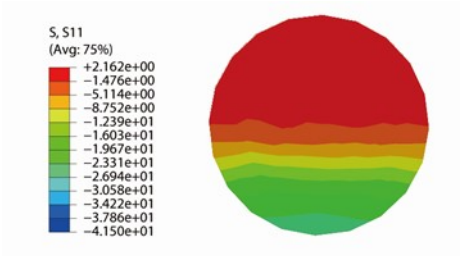

Fig.13 - The nephogram atlas of the concrete from S11 middle section of 1# test block in load 50KN.

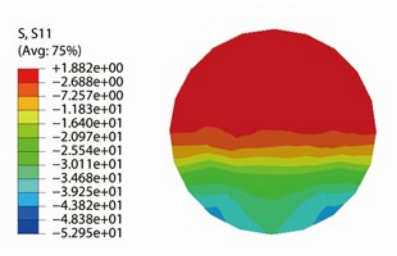

Fig.14 - The nephogram atlas of the concrete from S11 middle section of 1# test block in load 520KN.

In order to clarify the peeling and crack damage of the specimens, compared with the experiment the thickness-free cohesive element which is added to the simulation process. The stress-displacement rule is used to define the constitutive relation of the cohesive force unit, which is to describe the damage and evolution of the material. When the cohesive force unit reaches the broken strength, the cohesive force unit will be removed from the model and formed at the interface of the material unit. And then the material unit interacts with the penalty function through the algorithm.

The accurateness of the constitutive 100×100×100mm model of concrete is verified by uniaxial compression, which simulated the mechanical properties of concrete test block. The concrete block uses C3D4 linear tetrahedral element, while the cohesive uses COH3D6 element. Sweep the division of 19173 in total for each model, as shown in Figure 15. The simulated specimen is loaded by controlling the node displacement of the solid element on the top surface and the vertical displacement of the bottom of the simulated specimen is zero, which the loading method is similar to laboratory uniaxial compression.

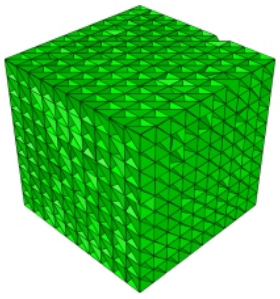

Fig. 15 - Test block mesh diagram.

4.5. Experimental test of single -axis compression of concrete cube test block

4.5.1. Test block production and conservation

With the same water-cement ratio of the preparation of concrete into 2 groups of 18 test pieces for the uniaxial compressive strength test, as shown in Figure 16. During the process of the test, followed by adding coarse, cement, admixture and water which mixed the test block evenly with mixer. The mixture was placed in a standard incubator (temperature 20±2℃, relative humidity>95%), and the mold was placed in a standard curing room.

4.5.2 Test method for uniaxial compressive strength of cubic test blocks

Cube compressive strength test which was in accordance with the "Ordinary Concrete Mechanical Properties Test Method Standards" (GB/T50081-2002) requirements, used with SANS servo hydraulic testing machine.

Fig.16 - Uniaxial compressive strength and splitting tensile strength test.

The compressive strength test load rate is among 0.5~0.8MPa/s[12-14], with C40 concrete during the continuous loading process of the test. When the specimen began to abruptly deformed and stopped loading in time until the test piece was destroyed, and recorded the breaking load as soon as possible. The compressive strength of the cube specimen was calculated and the compressive strength test was multiplied by the conversion factor of 0.95[15-16].

There are certain degrees of dispersion from the strength of the concrete, the measured data of the strength of the concrete cube in the laboratory which can not be directly used as a design standard. In the analysis of the test data, which wold be easy to use the intensity level corresponding to the standard value and design value for theoretical calculation.

The standard values for the strength of concrete can be expressed as:

$$f_k = f_m - 1.645\sigma \quad (5)$$

$$f_m = \frac{\sum_i^n f_{m,i}}{n}, \sigma = \sqrt{\frac{\sum_{i=1}^n f_i^2 - n\sum_{i=1}^n f_m^2}{n-1}} \quad (6)$$

Where: f_k is the standard value of concrete material strength; f_m is the average strength of concrete; σ is the material strength variance; n is the number of the same cube.

According to the above formula of (5) and (6), the indicators of the compressive strength in 0.4 water-cement ratio for test piece which are shown in Table 2.

Table 2

Parameters of concrete plastic damage model

Water-cement ratio	f_m/ MPa	σ MPa	f_k/ MPa
0.4	43.6 2	2.36	39.8

Through the ratio experiment, with the use of cement single dosage of 500kg and sand rate of 42%, which the C40 strength of this grade of concrete was successfully prepared. And the slump is more than 200mm which met the requirements of filling concrete as shown in Table 3.

The higher compressive strength of the concrete is, the smaller compressive deformation sustained will be. When reached the ultimate load, the concrete is suddenly destroyed and the brittleness is significant. Before the load reaches the peak intensity, there is no obvious crack on the surface of the test piece. After reached the peak intensity, the energy accumulated in the test block is quickly released and the crack is generated.

4.6. Comparison of experimental and simulated results

Taking the water-cement ratio of 0.4 as an example, the concrete axial compression data measured in the laboratory and the failure mode of the concrete axial pressure are compared with the simulation results. Compared with the displacement-load curves of the 4 typical concrete test blocks and the software simulation curve, which is in similar trend as shown in Figure 17.

Because the surface of the simulated uniaxial compression specimen is flat, however, the surfaces of the test specimens are rough, so it caused the similar trend between the simulated results and experiments.

Table 3

Normal concrete cube strength values with different water-cement ratio

Water cement ratio	Strength level	Material usage / kg.m^{-3}			Sand rate, %	Water reducing agent dosage, %	Slump mm	Slump expansion, mm
		cement	sand	stone				
0.4	C40	500	756	1044	42	0.2~0.3	220~240	620~640

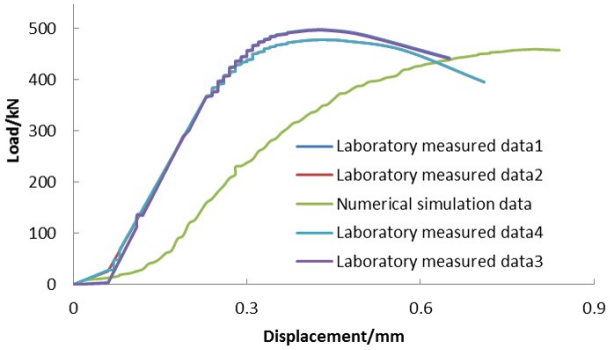

Fig. 17 - Uniaxial load displacement curve of concrete test block.

The deformation of the laboratory specimen at this stage is obviously larger than that of the numerical simulation analysis.

(1) As shown in Figure 18, the compression stage: When start loading, with the increase of displacement, the load of the specimen is not increased greatly. The deformation of the four specimens at this stage is: 0.62mm, 0.51mm, 0.47mm, 0.31mm. There are some micro-cracks in the surface of the concrete test block in the laboratory and the micro-pores are gradually be composted, as shown in Fig. 18(a). Meanwhile, during the simulation the axial pressure transmised from top to bottom and there is no deformation on entity unit, while the simulated specimen with cohesive element was compressed, which is shown in Fig.18 (b).

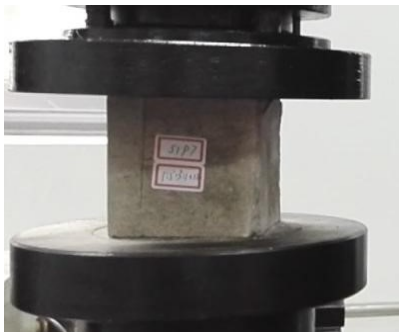

(a) Expansion of core concrete after compacting

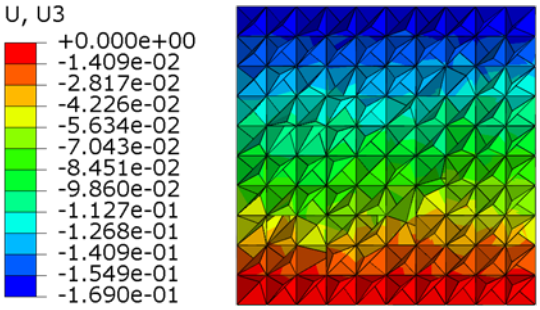

(b) Cohesive unit displacement cloud images

Fig.18 - Displacement cloud atlas of after test block compacting

(2) As shown in Figure 19, the elastic stage: with the axial load gradually increased, the deformation of the four specimens at this stage is: 0.63mm~0.99mm, 0.42mm~0.55mm, 0.27mm~0.5mm, 0.17mm~0.44mm during this stage. There are no obvious deformation on concrete entity units, but the some has begun to appear a small cracks. While the cohesive unit began to deform, which is similar to experimental results.

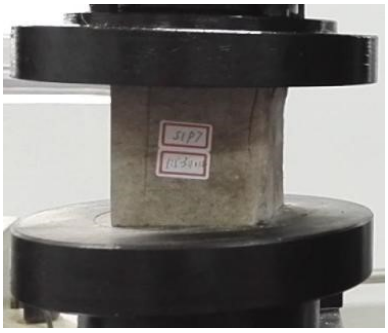

(a) Expansion of core concrete after elastic stage

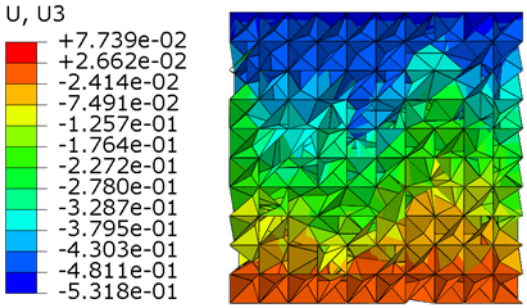

(b) Cohesive unit displacement cloud images

Fig.19 - Displacement cloud atlas of after elastic stage.

(3) As shown in Figure 20, the elastic-plastic stage: with the axial load gradually increased, the speed of the load is reduced. The deformation of the four specimens at this stage is: 0.99mm~1.15mm, 0.55mm~0.63mm, 0.57mm~0.78mm, 0.45mm~0.83mm during this stage. The surface of the concrete unit has produced a large number of tiny cracks, these tiny cracks would gradually go through the specimen within a wide range of lateral deformation, as shown in Fig. 20(a). The lower right corner of the specimen area in the physical unit, which has begun to slowly peel the test piece, no thickness of the bonding unit grid has been severely compressed, and gradually lost the ability to bond, as shown in Fig. 20(b).

(4) As shown in Figure 21, the destruction stage: with the plastic deformation of the specimen increases, the axial load is no longer increased. The deformation of the four specimens at this stage is: 1.35mm, 1.01mm, 1.19mm, 1.08mm, the specimen is completely destroyed. Most of the cracks on the surface of the specimen have been penetrated as sown in Fig. 21(a), and the concrete unit gradually begins to peel the specimen, the cohesive unit is squeezed severely, as shown in Fig. 21(b).

(a) Expansion of core concrete after elastic-plastic stage

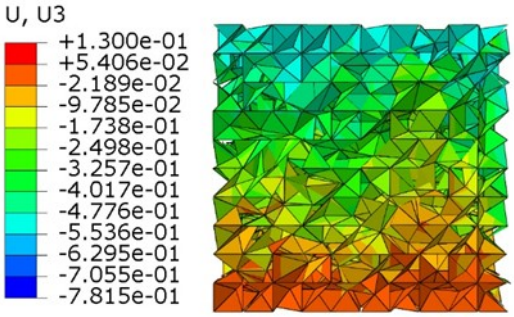

(b) Cohesive unit displacement cloud images

Fig.20 - Displacement cloud atlas of after elastic-plastic state

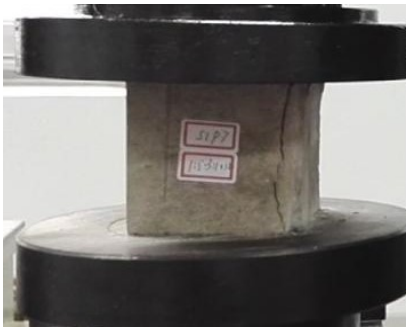

(a) Expansion of core concrete after destruction stage

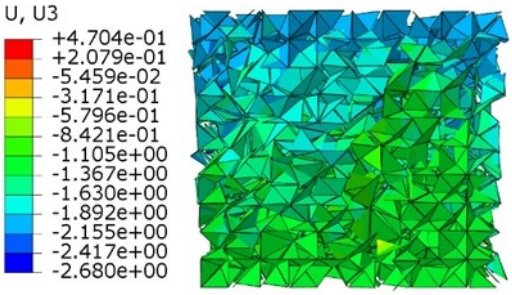

(b) Cohesive unit displacement cloud images

Fig.21 - Displacement cloud atlas of after destruction stage.

5. Monitoring of surface displacement of roadway surrounding rock

The observation includes the relative displacement of the arc middle section of the CFST arch as shown in Figure 22.

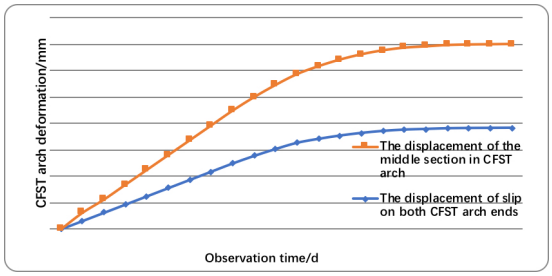

Fig.22 - Relative displacement monitoring curve of roadway surface

Since the CFST arch is supported by lining, so the largest relative displacement deformation of monitoring point is at the junction of the lining and the CFST arch. The relative displacement of the top plate and bottom plate is 115mm and 100mm, which meet the requirements of the stability from the surrounding rock of roadway. And the CFST arch is intact and non-significantly damaged then verify the superiority of CFST arch in the construction of roadway.

6.Conclusion

Through the bending test of the CFST arch in the large-scale laboratory, first, the displacement of the circular arc arch is monitored, and then, the load-displacement curve of the arc arch specimen is analyzed. In addition, the strain of outer wall from the steel pipe and the internal core concrete are monitored. Moreover, the failure process and the results of the single-axis compression test of the core concrete are compared with cohesive force bonding unit in ABAQUS which used into the damage morphology analysis.

(1) Through the experiment which shows that the internal of specimen will accumulate a lot of energy. And when the energy savings to a certain value, it needs to be released to the outside, so the specimen will be in the lateral deformation. If the process is developed in violent, the concrete will be horizontal "burst"; if not, the concrete will be gradual deformation in the horizontal direction.

(2) The distribution of the tension and compression zone of core concrete is analyzed. The early deformation of the steel pipe is reflected in the displacement meter. While the internal pores and cracks of core concrete are being gradually compacted under the axial pressure.

(3) The most of the cracks have been through the specimen and the entity unit which begin to peel from the model. Compared with the nephogram in ABAQUS with cohesive element which displayed accurately in the whole progress of uniaxial compression experiment in the micro aspects and the results are basically consistent. Therefore, the constitutive model of the CFST can be extended to other components of the concrete model used.

(4) The analysis of the stress distribution of the core concrete in the specimen, the core concrete deformation and the cause of the failure are summarized. the core concrete is locally stretched, in elastic deformation, and the cracks are produced inside, which resulting in the loss of part carrying capacity. As the load continues to increase, the local concrete with cracks will be expanded and crushed quickly, making the steel tube bulging and buckling, thus the drum occurred drum, buckling.

REFERENCES

1. W.F. Zhang, K.G. Chen, M.L. Li, et.al. Research and application of flexural behavior of concrete filled steel tubular support structure. Industrial Construction, 2016, **46**(1s), 962.
2. G.L. Qu G.L., PhD thesis. Research on Flexural Performance of Concrete-filled Steel Tubular Support and Its Application. Beijng: China University of Mining and Technology, 2015.
3. H. Li, W Wang. Application of ABAQUS secondary development in finite element analysis of concrete filled steel tubular structures. Journal of Building Structures, 2015, **34(8),** 353.
4. Y. Zhou, Z Li. A practical simulation platform of reinforced concrete fiber beam-column element. EngineeringMechanics,2016, **28**(4),102.
5. J. Han, Y. Li, W. Chen, et al. Development of concrete material subroutines based on ABAQUS three-dimensional beam element. Building Structure , 2015,**41** (5),111.
6. J. Nie, Wang Yuhang. Development and application of steel-concrete composite fiber beam model in ABAQUS platform. Engineering Mechanics, 2015, **29**(1),70.
7. T. Hibbitt, B. Karlsson, R. Sorensen. ABAQUS/Standard User Subroutines Reference Manual. USA: ThePennsylvania State University, 1998: 1.
8. H.T. Hu, C.S. Huang, M. H. Wu, et al. Nonlinear analysis of axially loaded concrete-filled tube columns with confinement effect. Journal of Structural Engineering, ASCE, 2015, **129 (**10),1322..
9. J.B. Mander, M.J. N. Priestley, R. Park. Theoretical stress-strain model for confined concrete. Journal of Structural Engineering ASCE, 1988, **114**(8),1804.
10. J. Shen, C. Wang, J Jiang. Reinforced concrete finite element and limit analysis of shell. Beijing: Tsinghua University Press, 1993,50.
11. X. Wang, X. Lu, L. Ye. Numerical simulation for the hysteresis behavior of RC columns under cyclic loads. Engineering Mechanic, 2007, **24** (12),76.
12. A. Esmaeily, Y. Xiao, Behavior of reinforced concrete columns under variable axial loads: analysis. ACI Structure Journal, 2016, **102** (5), 736.
13. F. Lgeron, P. Paultre, J. Mazar. Damage mechanics modeling of nonlinear seismic behavior of concrete structures. Journal of Structural Engineering, ASCE, 2015, **131** (6), 946.
14. L.H. Han, Y.F. Yang, Cyclic performance of concrete-filled steel CHS columns under flexural loading. Journal of Constructional Steel Research, 2015, **61**(4), 423.
15. F.J. Vecchio, M.P. Collins. The modified compression-field theory for reinforced concrete elements subjected to shear. ACI Structural Journal, 1986, **83**(2), 219.
16. L. Han, J. Yiou, Y. Yang. Behavior of concrete filled steel rectangular hollow sectional columns subjected to cyclic loading .China Civil Engineering Journal, 2016, **37(**11**),**11.

****

MANIFESTĂRI ȘTIINȚIFICE / SCIENTIFIC EVENTS

Sixth International Conference on Durability of Concrete Structures (ICDCS 2018), Leeds, UK, 18 – 20 July 2018

The International Conference on the Durability of Concrete Structures (ICDCS) series brings together leading experts in the field of concrete durability from around the world. The aim is to discuss recent progress and latest developments in materials technology, assessment of performance both in laboratories and on site, service life concepts and reuse and recycling of construction materials and products to enable concrete constructions to be durable and sustainable.

The general topics to be covered include:

- Influence of exposure environments on the durability
- Ionic/molecular transport and modelling
- Materials for enhancing the durability
- Mechanisms of deterioration
- Performance of deteriorated structures
- Design for durability and service life
- Life-cycle assessment of concrete structures
- Testing, inspection and monitoring methods
- Repair and maintenance
- Novel cementitious materials
- Practical applications

Contact: https://engineering.leeds.ac.uk/icdcs2018

****